18

Measuring Disorder in Graphene with Raman Spectroscopy

Ado Jorio[1], Erlon H. Martins Ferreira[2], Luiz G. Cançado[3], Carlos A. Achete[4] and Rodrigo B. Capaz[5]

[1,3]*Departamento de Física, Universidade Federal de Minas Gerais*
[2,4]*Instituto Nacional de Metrologia, Normalização e Qualidade Industrial*
[5]*Instituto de Física, Universidade Federal do Rio de Janeiro*
Brazil

1. Introduction

Since the experimental discovery of an easy method to produce graphene (Novoselov et al., 2004; 2005), there is a continuous rising of interest on this fascinating material. Due to its own peculiar electronic band structure, graphene is a promising material for the future electronic nanodevice industry. In any production process is of fundamental importance to control the quality of materials in a fast and non-destructive manner. Quantifying defects in graphene related systems is a major problem for the application of such materials (Neto et al., 2009).
In the field of carbon-based nanostructures, Raman spectroscopy has shown to be the most suitable technique since it accomplishes those desirable goals and also because it can be used to differentiate the many types of sp^2 carbon structures and to identify the presence of defects (Ferrari & Robertson, 2000; Pimenta et al., 2007). Defects are of great importance since they modify the electronic and optical properties of the system, sometimes in a desirable way. Raman spectroscopy is also one of the most sensitive techniques to probe disorder in carbon structures. The development of an accurate methodology to study disorder with Raman spectroscopy will certainly facilitate the control of the amount of induced disorder in a target system. By combining experiment and theory, a phenomelogical model has been established to explain the evolution of the Raman spectrum of graphene with increasing amount of disorder caused by low energy ion bombardment. Using this model one can extract information about the density of defects, the average defect size and also the Raman process relaxation length and its dependence with the laser excitation energy and temperature. How the ion bombardment procedure affects graphene samples with two or more layers and graphene read edges has also been studied.

2. Review of Raman spectroscopy in graphene-related systems

Graphene has two atoms in the unit cell and, therefore, six phonon branches. Three are acoustic branches and three are optical branches. From the three optical branches, one gives rise to an infra-red active mode at the Γ point, while the two other branches are degenerate at the Γ point and Raman active. Therefore, zone center ($q = 0$) phonons would generate a one peak Raman spectra. However, the electronic structure of graphene generates special

electron-phonon induced resonance conditions with non-zone center modes ($q \neq 0$), known in the literature as the double-resonance Raman scattering process. This double-resonance process is responsible for the graphene related systems to have a Raman spectra with many features (Saito et al., 2002; Thomsen & Reich, 2000).

Although the double resonance process can activate phonons from all the six branches, the main features in the Raman spectra of graphene come from the phonon branch related to the zone-center Raman-active mode, i.e. to the optical phonon branch related to in-plane stretching of the C-C bondings. The strongest Raman peaks in crystalline graphene are the so-called G (~1584 cm^{-1}) and G' (~2400-2800 cm^{-1}) bands. The first is the first-order Raman-allowed mode at the Γ point, and the second is a second-order Raman-allowed mode near the K point, activated by the double-resonance process. Furthermore, the presence of disorder in the crystalline lattice causes changes in the graphene Raman spectra, the most evident being the appearance of two new peaks, the so-called D (~1200-1400 cm^{-1}) and D' (1600-1630 cm^{-1}) bands. Both bands come from the in-plane optical branches (iTO and LO, respectively) and both are related to the double-resonance process. The D band comes from the iTO phonon near the K point, while the D' band comes from the LO phonon near the Γ point.

Since 1970, large efforts have been devoted to develop disorder-quantification methods using Raman spectroscopy for nano-graphite (Cançado et al., 2006; Ferrari & Robertson, 2000; Pimenta et al., 2007; Tuinstra & Koenig, 1970), carbon nanotubes (Chou et al., 2007; Hulman et al., 2005) and graphene (Jorio et al., 2010; Lucchese et al., 2010; Martins Ferreira et al., 2010; Teweldebrhan & Baladin, 2009). The most advanced protocols have been developed for the edge-defects in nano-graphite, where the in-plane crystallite dimensions ranging from $L_a = 20\,\text{nm}$ up to values larger than a microscope spot size can be obtained by measuring the intensity ratio between the disorder induced D band and the first-order allowed tangential G band, including the dependence of I_D/I_G with the excitation laser wavelength, as given by (Cançado et al., 2006)

$$L_a(\text{nm}) = (2.4 \times 10^{-10})\lambda_{laser}^4 (I_D/I_G)^{-1}. \quad (1)$$

Such behavior is shown in Figure 1. Equation 1 gives the state-of-the-art for using Raman spectroscopy to quantify nano-graphite crystallite sizes, which is related to a certain type of disorder that are the graphene edges. Of course the result given above is an averaged measure of all possible edge structures present in a bulk nanographite sample. It has been shown that the D band intensity depends on the atomic structure at the edge, and it is actually absent in graphite edges when the atomic structure exhibit the zigzag arrangement (Cançado et al., 2004). Figure 2 shows an example of a graphite edge. The atomic orientation of the lattice was identified with scanning tunnelling microscopy, thus showing that the armchair and zigzag orientations are parallel to edges 1 and 2 in Figure 2, respectively. This is consistent with the observed change in the D band intensity, but the observation of a small but non-null D band at edge 2 shows that the structure at the edge is not perfectly zigzag. This result has been used to identify zigzag vs. armchair edges in graphene as well (Neubeck et al., 2010), although up to date there is no evidence of perfect zigzag graphene edged. Such a perfect zigzag edge structure would be evidenced by the observation of a D' band in the Raman spectra with a complete absence of the D band (Cançado et al., 2004).

Finally, the picture discussed above does not hold for ion-bombarded induced defects in graphene samples, as shown by (Lucchese et al., 2010), because of the simple and fundamental geometric difference between defects related to the size of a nano-crystallite and point defects in the lattice, which changes the I_D/I_G dependence on the amount of disorder. Basically, the

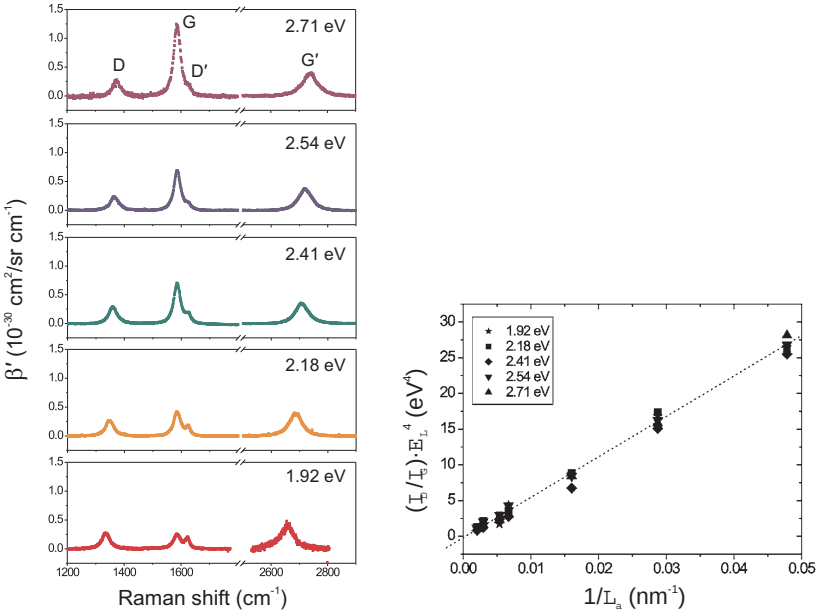

(a) (b)

Fig. 1. (a) The spectral differential cross section β' of the D, G, D', and G' bands for the nanographite sample with $L_a = 35$ nm, using five different values of E_L, each indicated at the top of the respective spectrum. The same vertical scale was used for the five spectra for comparison. (Cançado et al., 2007) (b) The intensity ratio I_D / I_G for nanographite samples normalized by E_L^4, plotted versus $1/L_a$ using five different laser excitation energies (Cançado et al., 2006).

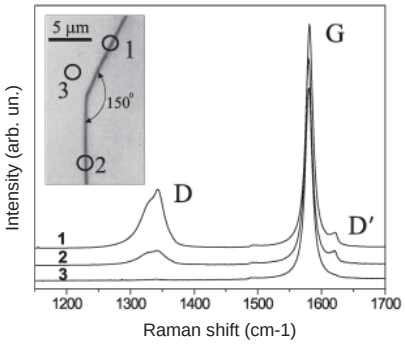

Fig. 2. Raman spectra obtained in three different regions of a highly oriented pyrolytic graphite (HOPG) sample. The inset shows an optical image of the step and the regions where spectra 1, 2, and 3 were taken (open circles). The atomic structure of the sample was identified using scanning tunneling microscopy, and the edges 1 and 2 were identified as parallel to the armchair and zigzag orientations, respectively. (Cançado et al., 2004)

disorder in a nano-crystallite can be quantified by the amount of border (one-dimensional defects) with respect to the total crystallite area, and this is a measure of the average inverse nano-crystallite size $1/L_a$. In ion bombarded graphene, the disorder is better quantified by the defect concentration, defined by $1/L_D^2$, where L_D is a typical interdefect distance, with the defect being a point-like (zero-dimensional) structure. In the following sections we will discuss these concepts in depth to develop the methods to quantify disorder in graphene related systems.

3. Creating defects on graphene by ion bombardment

There are many different techniques that could be used to investigate the amount of disorder in graphene, but Raman spectroscopy is certainly a fast and easy way to do it. However, to extract quantitative information from a Raman spectrum we need to calibrate the procedure. Such a calibration can be achieved with the help of a more direct technique such as scanning tunneling microscopy (STM), which can show the defects on the surface of a material. Doing STM on an exfoliated graphene is still a challenging task, since we need a graphene sample deposited on a conductive surface or make an electrical contact. The first method may complicate (if not prevent) to find the graphene on the surface and the second method can cause non-desirable defects on the sample (Ishigami et al., 2007; Neubeck et al., 2010). On the other hand, performing STM on graphite is a much simpler procedure, since the bulk graphite is conductive. One can then irradiate the graphite with low energy ions, do the STM image to count the number of defects per unit area and then perform the Raman measurement to correlate the relative intensity between the *D* and *G* bands with the measured ion dose. In a second step one can perform the same kind of irradiation on a graphene sample and use a HOPG flake as a reference for determining the actual ion dose (Lucchese et al., 2010).

Figure 3 shows STM images of a bulk HOPG surfaces, both pristine (a) and bombarded with 90 eV argon ions (b-e). Using the same parameters of current and ion energy, the increasing ion dose was obtained by increasing the bombardment time. From (b) to (e) the ion dose has been increased from 10^{11} Ar^+/cm^2 up to 10^{14} Ar^+/cm^2, which corresponds to an average distance between defects from $L_D = 32$ nm down to $L_D = 1$ nm. The right panel shows the Raman spectra measured for pristine HOPG and for the same HOPG right after each bombardment procedure shown in panels (b-e) (increasing bombardment dose from bottom to top). Although for the highest dose the HOPG surface seems already completely damaged, the Raman spectrum shows a well defined *G* band, indicating that the ions affect mostly the upper layers. To fully calibrate the bombardment procedure that is further going to be applied to the graphene samples, ion bombardment and consecutive Raman measurements on HOPG were performed three times, for up to eight different ion doses between 10^{11} and 10^{15} Ar^+/cm^2. The Raman response was measured at up to 7 locations within the HOPG specimen for each ion dose (Jorio et al., 2009).

Using this procedure, the same bombardment can be applied to a graphene sample. When obtaining a graphene sample by the micro-mechanical cleavage of graphite and further deposition on a SiO_2 substrate ("scotch tape" method), one can always find some bulk graphite flake next to a graphene sample. This small flake can then be used as a "standard" for the ion dose calibration by comparing its Raman spectrum with the previously HOPG measured spectrum discussed in Fig. 3. Thus one can skip the STM procedure on the graphene sample to actually count the number of defects on the sample. Figure 4(a) shows the Raman spectra of such a ion bombarded monolayer graphene subject to the same ion doses measured in the HOPG case. It is clear from those spectra that the graphene sample is much more

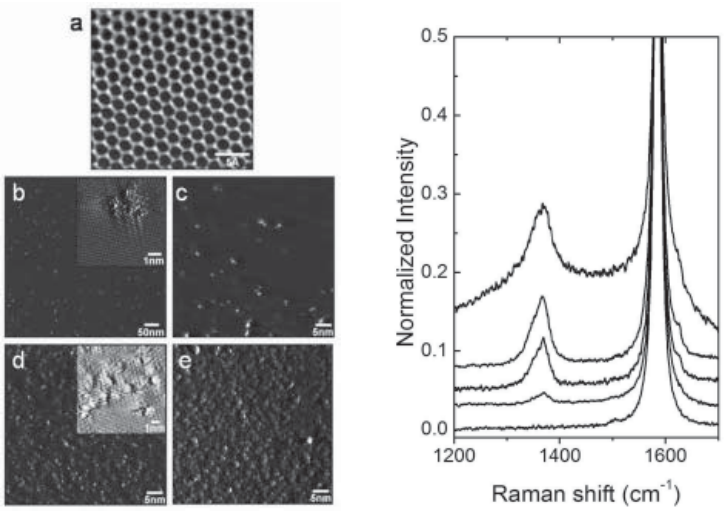

Fig. 3. Left panel are the STM images of (a) pristine HOPG surface and (b)–(e) after increasing ion bombardment showing how the defects are spread on the surface. (a) to (e) corresponds to zero, 10^{11}, 10^{12}, 10^{13}, 10^{14} Ar^+/cm^2 dose. Insets to (b) and (d) show some defects in detail. The right panel shows the Raman spectra of pristine HOPG and the same HOPG right after each bombardment in (a-e), increasing ion dose from bottom to top, showing the increasing *D* band.

sensitive to the ion bombardment procedure than the bulk graphite. Because it has just one layer, there is no extra contribution to the *G* band intensity as in the case of the inner layers of the HOPG sample. Then the relative intensity I_D/I_G increases up to ~ 3.5 in the monolayer case while it never reaches 1 in the HOPG sample, with an excitation laser energy of 2.41 eV ($\lambda = 514$ nm). A more complete behavior of those relative intensities can be seen in Figure 4(b). This graph shows the evolution of the relative intensity I_D/I_G with increasing ion dose (decreasing distance between defects) from 1.5×10^{11} to 2.5×10^{15} Ar^+/cm^2 (26 nm down to 0.63 nm) and compares with both the original Tuinstra-Koenig relation (Equation 1) for the graphite and a modified version introduced by (Lucchese et al., 2010). It is clear from the plot that Equation 1 does not hold for graphene because the topology of defects created by the ion bombardment is different from those boundaries defects. The relation introduced for point-like defects is (Lucchese et al., 2010).

$$\frac{I_D}{I_G} = \frac{C(\lambda)}{L_D^2}\,, \tag{2}$$

where, in this case, $C(514\text{ nm}) \sim 107\text{ nm}^2$. Still, the limit of validity of this relation is for the regime of low defect density (or $L_D > 6$ nm). In the graph we can see two well defined disorder regimes, one in the right side of the curve, which is the low disorder limit, and the one in the left side, which is typical of amorphous carbon structures. The complete model to describe the transition between the two regimes was described also in (Lucchese et al., 2010) and will be presented in Section 5.

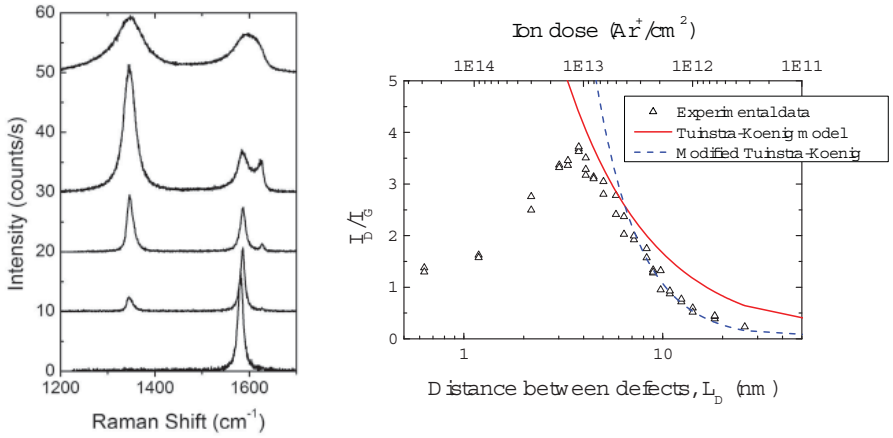

(a) (b)

Fig. 4. (a) Raman spectra of a monolayer graphene bombarded with low energy (90 eV) argon ions measured with a 514 nm laser. From bottom to top, curves correspond to zero, 10^{11}, 10^{12}, 10^{13} and 10^{14} Ar^+/cm^2 dose. (b) Comparison between experimental I_D/I_G data and both original and modified Tuinstra-Koenig relations for disorder in carbon structures (see text).

When studying disorder by means of Raman spectroscopy, the relative intensity between the D and G bands is the main feature that is taken into consideration. However, disorder is also responsible for the changes in the intensities of other bands, such as D' and G', and also affects the position and shape of the Raman peaks. Figure 5 plots the relative integrated areas of the main Raman bands, namely D, D' and G' with respect to G, and Figures 6(a) and 6(b) show the behaviour of the peak position and the full width at half maxium (FWHM) of those same bands for the same monolayer graphenes of Figure 4. A careful look at those plots shows that in the limit of low disorder (large L_D) there is no significant change in the peak position and just a slightly increase of the FWHM of all bands. However, for increasing disorder ($L_D \lesssim 4$ nm), there is an abrupt increase of the FWHM and also a small downshift in the peak positions. This suggests that even at moderately large disorder regimes, the C–C bonds are still sp^2 kind, with no significant strain in the bonds. When looking at the disorder in graphene, not only the ratio I_D/I_G must be considered, as it is clear that it is possible to have the same value of I_D/I_G for two different values of L_D. Therefore, it is important to look also at the values of the FWHM which can tell if the system is in lower or higher disorder regime.

4. Laser energy dependency

The experimental data presented in the previous Sections show that disorder introduced by a random distribution of defects causes significant changes in the relative intensities of the resonance Raman bands and it leads to broadening and shifting of those bands. Moreover, these effects appear to be strongly dependent on the laser excitation energy. It was a work by (Mernagh et al., 1984) that showed for the first time a strong dependency of the ratio I_D/I_G on the excitation laser energy E_L used in the Raman scattering experiment (Mernagh et al., 1984). Later on, (Cançado et al., 2006) measured the I_D/I_G ratio dependence on E_L for nanographites, and generated Equation 1.

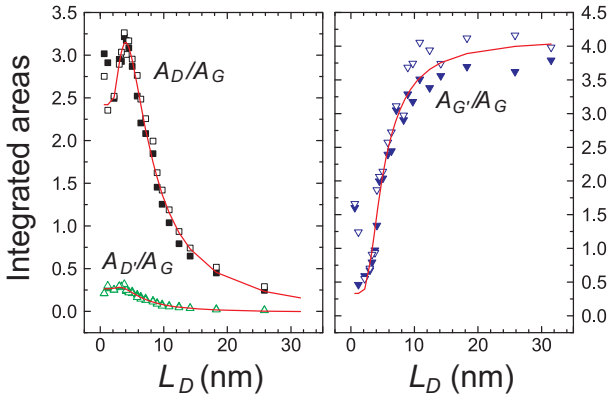

Fig. 5. Evolution of the integrated areas of the D, D' and G' bands normalized by the G band for a monolayer graphene bombarded with low energy argon ions. Symbols are the experimental data and the curves are the fitting with Equations 3 and 4. Open and filled symbols stand for two different graphene samples. (Martins Ferreira et al., 2010)

In this section we describe recent efforts to fully accomplish the protocol for quantifying the amount of point-like defects in graphene (or equivalently, L_D) (Cançado et al., 2011). For that, different excitation laser lines have been used for measuring the Raman spectra of ion bombarded samples with different L_D values and their respective I_D/I_G ratios.
Figures 7(a-c) show the Raman spectra of five distinct ion-bombarded graphene samples which were exposed to different ion bombardment doses in the range of 10^{11} Ar^+/cm^2 (one defect per 4×10^4 C atoms) to 10^{15} Ar^+/cm^2. The Raman spectra shown in panels (a), (b), and (c) were taken using the excitation laser energies (wavelengths) $E_L = 2.41$ eV ($\lambda_L = 514.5$ nm), $E_L = 1.96$ eV ($\lambda_L = 632.8$ nm), and $E_L = 1.58$ eV ($\lambda_L = 785$ nm), respectively. The samples have $L_D = 24$ nm, 14 nm, 7 nm, 5 nm and 2 nm. Figure 7(d) shows the Raman spectra of the ion-bombarded sample with $L_D = 7$ nm obtained using the three different laser energies. Notice that the ratio I_D/I_G decreases as the laser energy increases, showing that a complete analysis for the I_D/I_G ratio in graphene must take into account the excitation laser energy. However, before going into details, we have to introduce the model to analyse the evolution of the D and G peaks.

5. Theoretical model

5.1 The local activation model

A unified theoretical description of the disorder induced effects from a more fundamental point-of-view is still an open problem, although some advances have been made on the related problem of the D band arising from graphene edges (Basko, 2009; Casiraghi et al., 2009). Nevertheless, some understanding of the problem at hand has been achieved through phenomenological models, as we describe in this Section.
Both experiments (Cançado et al., 2006; Tuinstra & Koenig, 1970) and theory (Basko, 2009; Casiraghi et al., 2009) describe the D band as being "locally activated", i.e., it only becomes active in the near vicinity of an imperfection (such as an edge or a point defect). Therefore, for the specific case of disorder induced by impact of individual Ar^+ ions, we can associate a characteristic length scale r_A, measured from the impact point, as the typical decay distance

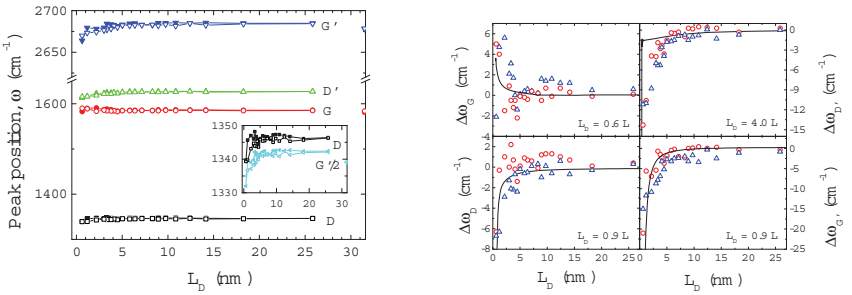

(a)

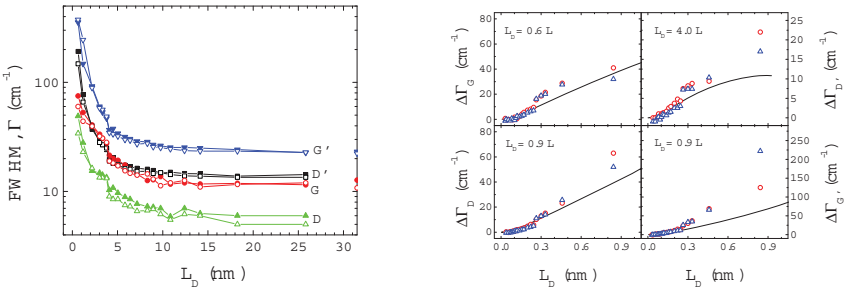

(b)

Fig. 6. Peak position (a) and full width at half maximum (b) of the four main Raman bands D, G, D' and G' of a monolayer graphene bombarded with low energy ions as a function of the average distance between the defects (L_D). Left panels show the absolute experimental data, and right panels the shifts in peak position and peak width with respect to the initial values (from the first bombardment). Symbols are experimental data and curves are the fitting from the theoretical model presented in Section 5. (Martins Ferreira et al., 2010)

of the D band intensity (green region in Figure 8). Another length scale is given by r_S, also measured from the impact points, which describes the region where the graphene sp^2 network disorganizes due to the ion impact (red region in Figure 8).

The activated region leads to an increase of the A_D/A_G ratio (equivalently on I_D/I_G), whereas the disorganized region reduces this ratio. By solving rate equations describing the evolution of the green and red regions with the ion dose, an analytical expression is obtained for A_D/A_G as a function of L_D (Lucchese et al., 2010; Martins Ferreira et al., 2010):

$$\frac{A_D}{A_G}(L_D) = C_A \frac{r_A^2 - r_S^2}{r_A^2 - 2r_S^2}\left[e^{-\frac{\pi r_S^2}{L_D^2}} - e^{-\frac{\pi(r_A^2 - r_S^2)}{L_D^2}}\right] + C_S\left[1 - e^{-\frac{\pi r_S^2}{L_D^2}}\right], \quad (3)$$

In this expression, the coefficients C_A and C_S correspond to the A_D/A_G ratio in two idealized limits. C_A refers to the situation in which the D band is activated in the whole of the graphene layer. Therefore, it embodies important information on the relative strengths

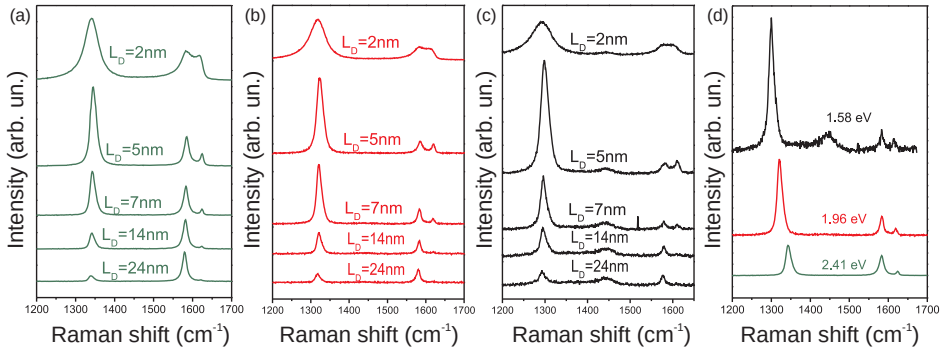

Fig. 7. (a-c) Raman spectra of five distinct ion-bombarded graphene samples using the excitation laser energies (wavelengths) E_L =2.41 eV (λ_L =514.5 nm), E_L =1.96 eV (λ_L =632.8 nm), and E_L =1.58 eV (λ_L =785 nm), respectively. (b) Raman spectra of an ion-bombarded sample with L_D = 7 nm obtained using the three different excitation laser energies. (Cançado et al., 2011)

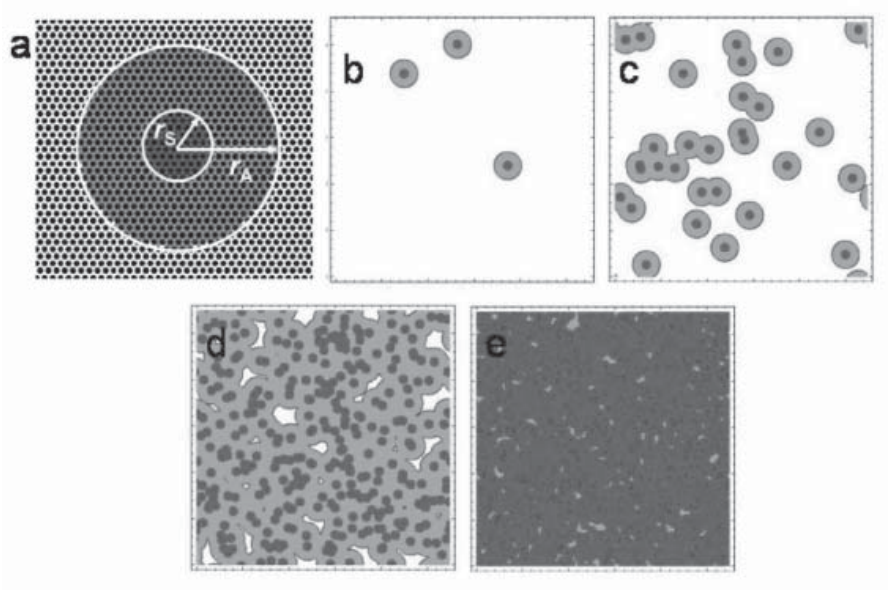

Fig. 8. (a) The two length scales (r_A and r_S) describing the evolution of the D band intensity with disorder induced by the impact of Ar^+ ions in graphene. Panels (b) to (e) correspond to the same ion doses in panels (b) to (e) in Figure 3. (Lucchese et al. (2010))

of the electron-phonon scattering near the Γ and K points in the Brillouin zone and on the electron-defect scattering cross-section for the D band. In particular, the strong energy dependence of C_A is revealing of the physics of Kohn anomaly near the K-point phonons in graphene (Piscanec et al., 2004) and of electron-defect scattering on short-range imperfections of graphene (Basko, 2008). The coefficient C_S corresponds to the A_D/A_G ratio in the highly disordered limit.

Notice from Figure 5 that this analytical function describes the experimental evolution of A_D/A_G with the amount of disorder, including its energy dependence. Moreover we can also extract physical meaning from the two length scales obtained from the fits. For instance r_S appears to be energy-independent, which is consistent with its interpretation as geometrical, structure-related length. The fitted values of r_S are in accordance with the typical defect-size estimates found from STM analysis (Martins Ferreira et al., 2010), which shows a sparse size distribution with an average value of 1.8 nm. The length $r_A - r_S$ is a rough measure of the length traveled over the lifetime of the electron-hole pair, v_F/ω_D, where v_F is the graphene Fermi velocity (Casiraghi et al., 2009). This length is energy-dependent, as imposed by the double-resonance condition and the strong phonon dispersion near the K point.

The analytical function in Equation 3 also describes the evolution of D' band integrated area with disorder (Martins Ferreira et al., 2010). Similar ideas can be applied for the $A_{G'}/A_G$ ratio. However, the G' band is already active for pristine graphene, so the integrated area ratio is only affected by the progressive disorganization of the graphene network, leading to:

$$\frac{A_{G'}}{A_G}(L_D) = \frac{A_{G'}}{A_G}(\infty) - B\left[1 - \mathrm{e}^{-\frac{\pi r_S^2}{L_D^2}}\right], \tag{4}$$

where $A_{G'}/A_G(\infty)$ is the area ratio for pristine graphene. The fitting of the experimental data also shows an excellent agreement in this case.

5.2 The excitation energy dependence

Now we can consider the excitation energy dependence in more depth. Figure 9(a) shows the I_D/I_G data (bullets) for all graphene samples and laser energies used in the experiment. The lines are the fitting curves following Equation 3. The C_A values obtained from the fitting shown in Figure 9(a) are plotted in the inset to Figure 9(a) (down triangles). Notice that C_A decrease as the laser energy increases. This behavior is ruled by a strong dependency of the strength of the D band on the wavevector of phonons involved in the double-resonance scattering process (Cançado et al., 2011). The solid line in the inset to Figure 9(a) is the fitting of the experimental data using an inverse fourth power dependence on the excitation laser energy, which gives $C_A = 140\,E_L^{-4}$, following the results on nanocrystallites (Cançado et al., 2006). This dependence is not yet understood and may be restricted to this energy range.

Although C_S could present some dependency with the excitation laser energy, our experimental data set does not allow us a clear determination of this dependency. In this case, we have considered $C_S = 0.9$ for all three excitation laser energies used in the experiment, in agreement with the more detailed results displayed in Figure 4(b). The fitting also gives $r_A = 3.1$ nm, and $r_S = 1$ nm, which is in excellent agreement with the values obtained by (Lucchese et al., 2010) and (Beams et al., 2010).

Figure 9(b) shows the plot of the product $E_L^4(I_D/I_G)$ versus L_D for the experimental data shown in Figure 9(a). It is clear from the plot depicted in Figure 9(b) that the data with $L_D > 10$ nm obtained with different laser energies collapse in the same curve. The same is not valid for

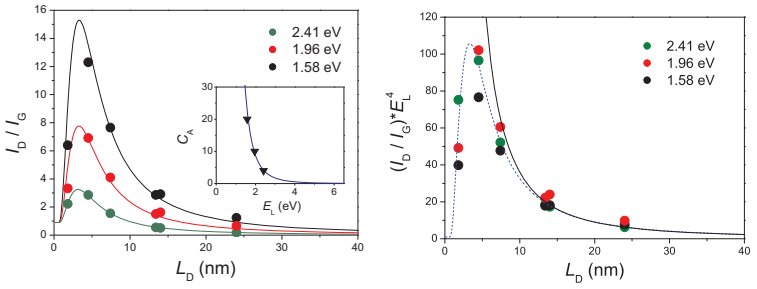

Fig. 9. (a) I_D/I_G data (bullets) for all graphene samples and laser energies used in the experiment. The solid lines are the fitting curves according to Equation 3. The inset shows the plot of C_A versus E_L. (b) Plot of the product $(I_D/I_G)E_L^4$ versus L_D for the experimental data shown in Figure 9(a). (Cançado et al., 2011)

$L_D < 10$ nm, indicating that C_S might also play a role in the E_L dependence. The dashed blue line is the plot obtained from the substitution of the relation $C_A = 140/E_L^4$ in Equation 3.
We now turn our attention to the low defect density regime ($L_D \geq 10$ nm). In this regime, for which $L_D > 2r_A$, the total area contributing to the D band scattering is simply proportional to the number of point defects, giving rise to $I_D/I_G \propto 1/L_D^2$ (see Equation 2). By considering large values of L_D, and also taking in account that $C_A(r_A^2 - r_S^2) \gg C_S r_S^2$, Equation 3 takes the form

$$\left(\frac{I_D}{I_G}\right) \simeq C_A \frac{\pi(r_A^2 - r_S^2)}{L_D^2}. \tag{5}$$

By taking the values $r_A = 3.1$ nm, $r_S = 1$ nm, and also the relation $C_A = 140/E_L^4$ obtained from the fit of the experimental data shown in Figure 9(a), Equation 5 can be rewritten as

$$L_D^2(\text{nm}^2) = \frac{3600}{E_L^4}\left(\frac{I_D}{I_G}\right)^{-1}. \tag{6}$$

The above relation is valid for Raman data obtained from graphene samples that present point defects with $L_D \geq 10$ nm using excitation laser lines in the optical range. In terms of the defect density $n_D(\text{cm}^{-2}) = 10^{-14}/L_D^2$, Equation 6 becomes

$$n_D(\text{cm}^{-2}) = (2.8 \times 10^{-18})E_L^4\left(\frac{I_D}{I_G}\right). \tag{7}$$

The solid dark line in Figure 9(b) is the plot of the product $E_L^4(I_D/I_G)$ versus L_D according to Equation 6. The plot shown in Figure 9(b) clearly validates this relation for samples with $L_D > 10$ nm.

5.3 Evolution of peak frequency and width

The evolution of the Raman FWHM and frequency shifts with increasing disorder in graphene can also be described by a phenomenological model, the so-called "spatial-correlation model". This model was originally developed to describe the evolution of the Raman spectra of disordered semiconductors (Richter et al., 1981; Tiong et al., 1984). In a crystalline system,

the Raman intensity $I_0(\omega)$ associated to a vibrational mode of wavevector $\mathbf{q}_0$ and frequency $\omega(\mathbf{q}_0)$ is described by a Lorentzian:

$$I_0(\omega) \propto \frac{1}{[\omega - \omega(\mathbf{q}_0)]^2 + [\Gamma_0/2]^2}, \tag{8}$$

where the FWHM Γ_0 is the inverse phonon lifetime. In a perfect system, Γ_0 has contributions from both electron-phonon and phonon-phonon (anharmonic effects) interactions. A disordered distribution of point defects will add a contribution to the FWHM by coupling phonons of different momenta, so the phonon wave packet in k-space can be described by a Gaussian function $\exp[-(\mathbf{q} - \mathbf{q}_0)^2 L^2/4]$ centered in $\mathbf{q}_0$ and having a width proportional to $1/L$. In real space, L is a measure of the phonon coherence length, which should be a good measure of the average distance between point defects. Then, the Raman intensity for the disordered graphene $I(\omega)$ is written as (Tiong et al., 1984):

$$I(\omega) \propto \int_{BZ} d^2q \frac{W(\mathbf{q}) \exp\left[\frac{-(\mathbf{q}-\mathbf{q}_0)^2 L^2}{4}\right]}{[\omega - \omega(\mathbf{q})]^2 + [\Gamma_0/2]^2}, \tag{9}$$

where, in our case, the integral is taken over the two-dimensional graphene Brillouin Zone and $W(\mathbf{q})$ is a weighting function that describes wavevector dependence of the electron-phonon coupling for the Raman process.

Within this phenomenological model, and using experimentally available phonon dispersion relations the full lineshape of $I(\omega)$ can be calculated, and from that the disorder-induced peak shifts $\Delta\omega_{\mathbf{q}_0}$ and the increase in FWHM $\Delta\Gamma_{\mathbf{q}_0}$ can be extracted. Details of the application of this model to specific Raman bands can be found in (Martins Ferreira et al., 2010). As seen in Figures 6(a) and 6(b), this simple model describes the main qualitative features of experimental data on the evolution of the FWHM and peak-frequency shifts of the D, D', G and G' bands with disorder. Notice that the agreement is better for large values of L_D, as expected. In the figures, we also show the best relationships between L and L_D in each case (obtained by the fits). Notice that L and L_D are similar to each other and this behavior arises naturally from the fitting procedure. That means the disordered-induced phonon coherence length is of the same order of the typical inter-defect distance, as we argued. Also, it seems that the D' modes are the most affected by disorder, showing a smaller coherence length than the other modes for the same amount of disorder. Finally, the model allows us to explain the greater increase in FWHM of the modes near K with respect to the modes near Γ as simply a consequence of the larger magnitude of phonon dispersions near K.

6. Effect of ion bombardment on few-layer graphenes

Differently from the monolayer, where the G' and D bands are described by a single Lorentzian function, in a graphene with 2 or more layers, those bands become more complex due to the interaction between the layers, and, therefore, a quantitative description of the evolution of the Raman bands with increasing disorder is a tougher task (Martins Ferreira et al., 2010). Figure 10 shows the Raman spectra of a bilayer and a trilayer graphene sample subjected to the same ion bombardment of the previously discussed monolayer sample. In comparison, the effect of ion bombardment in this sample is less pronounced than in monolayer. The I_D/I_G ratio grows faster and reaches a higher value for the monolayer than for the bilayer, and the same applies to the bilayer as compared to the trilayer. This behavior is a confirmation that the defects are mainly on the surface (Jorio et al., 2010). Since the Raman

signal gets the contribution of all the layers, the *G* band intensity must be stronger for the bilayer and trilayer, while the *D* band intensity, which depends mostly on the number of defects, must be approximately the same. This can explain the behavior of the intensity ratios I_D / I_G. As for the case of the monolayer, we see no significant change in the frequency of the *G* band, and we observe a broadening of the peaks for the higher ion doses (Martins Ferreira et al., 2010).

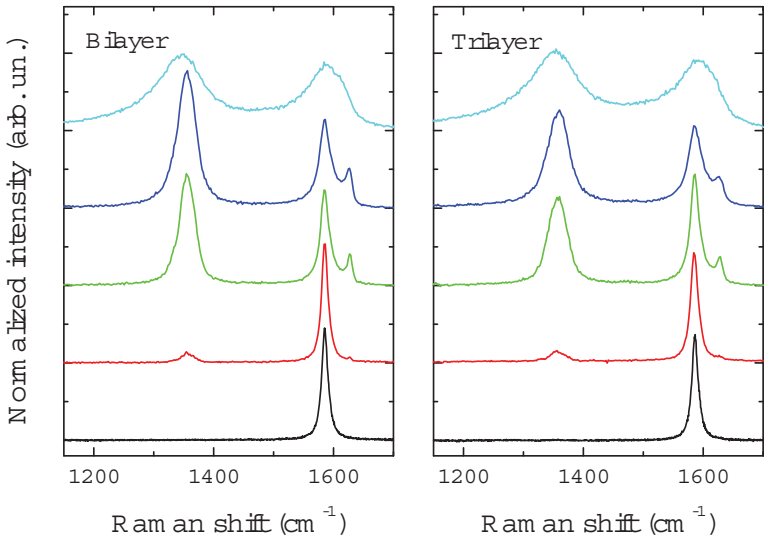

Fig. 10. Raman spectra of bilayer and trilayer graphenes bombarded with low energy (90 eV) argon ions. From bottom to top, curves correspond to zero, 10^{11}, 10^{12}, 10^{13} and 10^{14} Ar^+/cm^2 doses. (Jorio et al., 2010)

7. Raman at edges

The borders of a graphene sheet act like defects in the crystallographic structure and may have great impact in transport properties of graphene. As discussed in Section 2, previously studies on graphite edges have shown that the Raman *D* band intensity depends on the crystallographic orientation of the edge and the polarization of the laser beam (Cançado et al., 2004). Figure 11 shows the Raman mapping of the *D* band of a graphene sample showing the presence of defects at the borders (Carozo et al., 2011). For graphene, it has also been shown that the intensity of the *D* band is stronger for an incident light with polarization parallel to the border and is proportional to $\cos^2 \theta$, where θ is the angle between the polarization of incident light and the edge (Casiraghi et al., 2009; Gupta et al., 2009). Theoretically it is expected that the *D* band intensity would vanish for a perfectly oriented edge, such as armchair or zigzag, when the incident light polarization is perpendicular to the edge. However, both (Casiraghi et al., 2009) and (Gupta et al., 2009) failed to found a null *D* band intensity with

a perpendicular polarization and they could not tell the difference between the a zigzag and armchair borders by the evaluation of the relative intensity I_D / I_G, contrary to what have been found by (Cançado et al., 2004). The conclusion was that the edges were not a perfect zigzag or armchair, but a mix of them. A more recent work by (Neubeck et al., 2010) determined the crystallographic orientation of a graphene sheet by STM measurements and found that the intensity of the *D* band is higher for the armchair edge than for the zigzag edge when the polarization of the laser beam was parallel to the edges, in accordance with have been published by (Cançado et al., 2004). Yet, it is expected that a perfect zigzag border would not present a *D* band, due to phonon momentum conservation (Cançado et al., 2004). It is to conclude then, that although at a microscopy level the border may be mainly zigzag or armchair, at the atomic level it is not perfect.

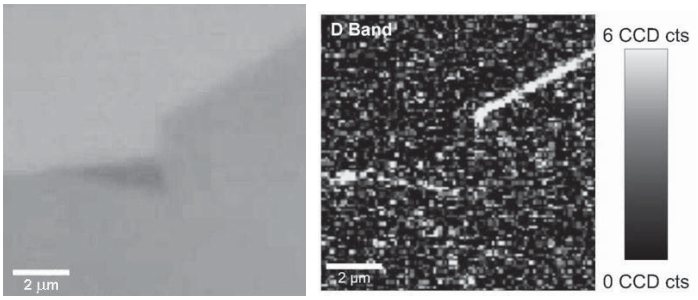

(a) (b)

Fig. 11. (a) Optical image of a monolayer graphene and (b) the Raman mapping of the *D* band of the same graphene sample showing the presence of the defects at the border (Carozo et al., 2011).

Finally, a theoretical work of (Sasaki et al., 2010) proposed that the intensity of the *G* band at the edges may be different depending on the orientation of the border, however no experimental data has corroborated it so far. The major difficulty in these studies to the moment is to obtain a perfect zigzag or armchair edge in sample produced by micro-mechanical cleavage. It is expected that graphene samples produced via chemical exfoliation may produce a much smoother edge and then those theories could be tested.

8. Conclusions and perspectives

The possibility of performing experiments on an isolated graphene sample improved substantially our understanding of disorder-induced effects in the Raman spectra of graphene related systems, even though such effects have been studied since 1970. Performing joint spectroscopy and microscopy experiments on a single layer of atoms allowed us to have a clear picture of the disorder effect in both real and reciprocal spaces, setting us free from volume-related aspects that were not easily addressable by microscopy and depend on light penetration depth. The parameters ruling the intensity of disorder-induced Raman bands, named r_A, r_S, C_A, C_S and defect topology, are now clearly established, so that accurate models can be developed for fully understanding the importance of electron-phonon and electron-defect interactions in this matter. The evolution of peak frequencies and linewidths are also clearly understood now for the low disorder limit, as discussed in this chapter. However, for understanding the peak behavior at the large disorder limit, more experimental

and theoretical developments are needed. Finally, all this development has shown that, up to date, no perfect zigzag graphene edge has been produced. Edge perfection will be important for the electronic properties of graphene nanoribbons, and Raman spectroscopy might play an important role on testing the development of such edges.

9. References

Basko, D. M. (2008). Resonant low-energy electron scattering on short-range impurities in graphene, *Phys. Rev. B* 78: 115432.

Basko, D. M. (2009). Boundary problems for dirac electrons and edge-assisted Raman scattering in graphene, *Phys. Rev. B* 79: 205428.

Beams, R., Cançado, L. G. & Novotny, L. (2010). Optical measurement of the phase-breaking length in graphene. arXiv:1008.1563v.

Cançado, L. G., Jorio, A., Martins Ferreira, E. H., Stavale, F., Achete, C. A., Moutinho, M. V. O., Capaz, R. B., Lombardo, A. & Ferrari, A. C. (2011). Laser energy dependency of the disorder-induced band in the Raman spectrum of graphene. Umpublished.

L. G., Takai, K., Enoki, T., Endo, M., Kim, Y. A., Mizusaki, H., Jorio, A., Coelho, L. N., Magalhães-Paniago, R. & Pimenta, M. A. (2006). General equation for the determination of the crystallite size L_a of nanographite by Raman spectroscopy, *Applied Physics Letters* 88(16): 163106.

Cançado, L. G., Jorio, A. & Pimenta, M. A. (2007). Measuring the absolute Raman cross section of nanographites as a function of laser energy and crystallite size, *Phys. Rev. B* 76(6): 064304.

Cançado, L. G., Pimenta, M. A., Neves, B. R. A., Dantas, M. S. S. & Jorio, A. (2004). Influence of the atomic structure on the Raman spectra of graphite edges, *Phys. Rev. Lett.* 93(24): 247401.

Carozo, V., Almeida, C. M., Martins Ferreira, E. H., Achete, C. A., Jorio, A. (2011). Raman Spectroscopy of Folded Graphene. Umpublished.

Casiraghi, C., Hartschuh, A., Qian, H., Piscanec, S., Georgi, C., Fasoli, A., Novoselov, K. S., Basko, D. M. & Ferrari, A. C. (2009). Raman spectroscopy of graphenes edges, *Nano Lett.* 9(4): 1433–1441.

Chou, S. G., Son, H., Kong, J., Jorio, A., Saito, R., Zheng, M., Dresselhaus, G., & Dresselhaus, M. S. (2007). Length characterization of DNA-wrapped carbon nanotubes using Raman spectroscopy, *Appl. Phys. Lett.* 90: 131109.

Ferrari, A. C. & Robertson, J. (2000). Interpretation of Raman spectra of disordered and amorphous carbon, *Phys. Rev. B* 61(20): 14095–14107.

Gupta, A. K., Russin, T. J., Gutiérrez, H. R. & Eklund, P. C. (2009). Probing graphene edges *via* Raman scattering, *ACS Nano* 3(1): 45–52.

Hulman, M., Skakalova, V., Roth, S. & Kuzmany, H. (2005). Raman spectroscopy of single-wall carbon nanotubes and graphite irradiated by γ rays, *J. of Appl. Phys.* 98(2).

Ishigami, M., Chen, J. H., Cullen, W. G., Fuhrer, M. S. & Williams, E. D. (2007). Atomic structure of graphene on SiO_2, *Nano Letters* 7(6): 1643–1648.

Jorio, A., Lucchese, M. M., Stavale, F. & Achete, C. A. (2009). Raman spectroscopy study of Ar^+ bombardment in highly oriented pyrolytic graphite, *Phys. Status Solidi B* 246(11–12): 2689–2692.

Jorio, A., Lucchese, M. M., Stavale, F., Martins Ferreira, E. H., Moutinho, M. V. O., Capaz, R. B. & Achete, C. A. (2010). Raman study of ion-induced defects in N-layer graphene, *J. Phys.: Condens. Matter* 22: 334204.

Lucchese, M. M., Stavale, F., Martins Ferreira, E. H., Vilani, C., Moutinho, M. V. O., Capaz, R. B., Achete, C. A. & Jorio, A. (2010). Quantifying ion-induced defects and Raman relaxation length in graphene, *Carbon* 48(5): 1592–1597.

Martins Ferreira, E. H., Moutinho, M. V. O., Stavale, F., Lucchese, M. M., Capaz, R. B., Achete, C. A. & Jorio, A. (2010). Evolution of the Raman spectra from single-, few-, and many-layer graphene with increasing disorder, *Phys. Rev. B* 82(12): 125429.

Mernagh, T. P., Cooney, R. P. & Johnson, R. A. (1984). Raman spectra of graphon carbon black, *Carbon* 22(1): 39–42.

Neto, A. C., Guinea, F., Peres, N. M. R. & Geim, K. S. N. A. K. (2009). The electronic properties of graphene, *Rev. Mod. Phys.* 81: 109–162.

Neubeck, S., You, Y. M., Ni, Z. H., Blake, P., Shen, Z. X., Geim, A. K. & Novoselov, K. S. (2010). Direct determination of the crystallographic orientation of graphene edges by atomic resolution imaging, *Appl. Phys. Lett.* 97(5): 053110.

Novoselov, K. S., Geim, A. K., Morozov, S. V., Jiang, D., Zhang, Y., Dubonos, S. V., Grigorieva, I. V. & Firsov, A. A. (2004). Electric field effect in atomically thin carbon films, *Science* 306(666–669).

Novoselov, K. S., Jiang, D., Schedin, F., Booth, T. J., Khotkevich, V. V., Morozov, S. V., & Geim, A. K. (2005). Two-dimensional atomic crystals, *Proc. Natl. Acad. Sci. USA* 102(30): 10451–10453.

Pimenta, M. A., Dresselhaus, G., Dresselhaus, M. S., Cançado, L. G., Jorio, A. & Saito, R. (2007). Studying disorder in graphite-based systems by Raman spectroscopy, *Physical Chemistry Chemical Physics* 9: 1276–1291.

Piscanec, S., Lazzeri, M., Mauri, F., Ferrari, A. C. & Robertson, J. (2004). Kohn anomalies and electron-phonon interaction in graphite, *Phys. Rev. Lett.* 93(18): 185503.

Richter, H., Wang, Z. P. & Ley, L. (1981). The one phonon Raman spectrum in microcrystalline silicon, *Solid State Commun.* 39: 625.

Saito, R., Jorio, A., Filho, A. G. S., Dresselhaus, G., Dresselhaus, M. S. & Pimenta, M. A. (2002). Probing phonon dispersion relations of graphite by double resonance Raman scattering, *Phys. Rev. Lett.* 88(02): 027401.

Sasaki, K., Saito, R., Wakabayashi, K. & Enoki, T. (2010). Indentifying the orientation of edge of graphene using G band Raman spectra, *J. of the Phys. Soc. of Japan* 79(4): 044603.

Teweldebrhan, D. & Baladin, A. A. (2009). Modification of graphene properties due to electron-beam irradiation, *Appl. Phys. Lett.* 94: 013101.

Thomsen, C. & Reich, S. (2000). Double resonant Raman scattering in graphite, *Phys. Rev. Lett.* 85(24): 5214.

Tiong, K. K., Amirtharaj, O. M., Pollak, F. H. & Aspnes, D. E. (1984). Effects of as^{+} ion implantation on the Raman spectra of GaAs: spatial correlation interpretation, *Appl. Phys. Lett.* 44: 122.

Tuinstra, F. & Koenig, J. L. (1970). Raman spectrum of graphite, *J. Chem. Phys.* 53(3): 1126–1130.